*Catalysts* **2015**, *5*, 1034-1045; doi:10.3390/catal5031034

OPEN ACCESS

*catalysts*

**ISSN 2073-4344**

www.mdpi.com/journal/catalysts

*Article*

# Polyaniline-Derived Ordered Mesoporous Carbon as an Efficient Electrocatalyst for Oxygen Reduction Reaction

**Kai Wan, Zhi-Peng Yu and Zhen-Xing Liang ***

Key Laboratory on Fuel Cell Technology of Guangdong Province, School of Chemistry and Chemical Engineering, South China University of Technology, Guangzhou 510641, China;
E-Mails: wankai_scut@yeah.net (K.W.); yuzhipeng_scut@yeah.net (Z.-P.Y.)

* Author to whom correspondence should be addressed; E-Mail: zliang@scut.edu.cn; Tel./Fax: +86-20-8711-3584.

Academic Editor: Minhua Shao

*Received: 12 May 2015 / Accepted: 19 June 2015 / Published: 26 June 2015*

**Abstract:** Nitrogen-doped ordered mesoporous carbon was synthesized by using polyaniline as the carbon source and SBA-15 as the template. The microstructure, composition and electrochemical behavior were extensively investigated by the nitrogen sorption isotherm, X-ray photoelectron spectroscopy, cyclic voltammetry and rotating ring-disk electrode. It is found that the pyrolysis temperature yielded a considerable effect on the pore structure, elemental composition and chemical configuration. The pyrolysis temperature from 800 to 1100 °C yielded a volcano-shape relationship with both the specific surface area and the content of the nitrogen-activated carbon. Electrochemical tests showed that the electrocatalytic activity followed a similar volcano-shape relationship, and the carbon catalyst synthesized at 1000 °C yielded the best performance. The post-treatment in $NH_3$ was found to further increase the specific surface area and to enhance the nitrogen doping, especially the edge-type nitrogen, which favored the oxygen reduction reaction in both acid and alkaline media. The above findings shed light on electrocatalysis and offer more strategies for the controllable synthesis of the doped carbon catalyst.

**Keywords:** ammonia-activation; electrocatalysis; fuel cells; nitrogen-doped mesoporous carbon; oxygen reduction reaction

## 1. Introduction

The oxygen reduction reaction (ORR) is one key electrochemical process for the energy conversion devices, like fuel cells and metal-air batteries. Pt-based materials have been so far acknowledged to be the most effective catalysts for the ORR at low temperatures [1,2]; however, the source scarcity and high cost pose great challenges to the large-scale applications to fuel cells [3–5]. Hence, enormous effort has been devoted to search for greater efficiency, durability and less cost [6,7].

In recent years, nanostructured carbon materials have attracted increasing attention as the Pt-alternative electrocatalysts. Dai [8] synthesized 1D nitrogen-doped carbon nanotubes by the chemical vapor deposition (CVD) method with iron (II) phthalocyanine as the precursor, which featured high charge transfer and, thus, facilitated the ORR. Feng [9] synthesized 2D graphene-based carbon nitride nanosheets, of which the high specific surface favored the dense assembling of the active sites on the surface. Lu [10] synthesized 3D hierarchically porous nitrogen-doped carbons with a hieratical porous structure, which enabled low mass transfer resistance and improved accessibility of catalytic sites for the ORR.

Among them, nitrogen-doped ordered mesoporous carbon (NOMC) features high specific surface area and a uniform pore structure, which respectively facilitate the reaction kinetics and mass transfer to the electrode [11,12]. The hard-template method is a universal strategy to synthesize such materials, and SBA-15 is one of the most often used templates to synthesize NOMCs. Asefa [13] synthesized NOMC catalysts by pyrolyzing polyaniline in the framework of SBA-15. It was found that the NOMC catalyst pyrolyzed at 800 °C showed the best ORR performance. Guo [14] synthesized a series of NOMC catalysts with honey as the precursor, which showed a high specific surface area ranging from 1050 to 1273 $m^2 \cdot g^{-1}$. Mullen [15] synthesized high-performance NOMC catalysts by pyrolyzing ionic liquid within SBA-15. All of the above-mentioned catalysts showed a decent electrocatalytic activity to the ORR in alkaline media. Other mesoporous silicas have been also used for the synthesis. For example, Popov [16] synthesized nitrogen-doped ordered porous carbon with the aid of SBA-12, which also showed a superior activity for the ORR. Joo [17] synthesized a series of carbon catalysts by using various templates, like SBA-15, MSU-F, KIT-6 and fumed Carb-O-sil M-5. It was found that the template SBA-15 yielded an extremely high surface area of 1500 $m^2 \cdot g^{-1}$ and the best electrocatalytic activity.

Beside the template, the carbon precursor has a considerable effect on the microstructure and composition of the final carbon materials. A variety of nitrogen-containing organic chemicals, like phthalocyanine [18], porphyrin [19,20] and ionic liquid [21,22], have been used as the carbon precursor to synthesize the nitrogen-doped carbon catalyst. Polyaniline represents an aromatic ring connected via nitrogen-containing groups and, thus, facilitates the incorporation of nitrogen-containing active sites into the carbon matrix during the heat treatment [23]. Zelenay [23] found that the polyaniline-derived carbon electrocatalyst showed a superior performance to the ORR, which exhibited the highest maximum power density of 0.55 $W \cdot cm^{-2}$ at 0.38 V.

It has been well acknowledged that the template, carbon precursor and pyrolysis conditions have significant and complicated effects on the composition, structure and electrocatalytic activity of the ORR. In our previous work, we developed a method to synthesize the nitrogen-doped ordered mesoporous carbon featuring a high specific surface area [24,25]. Additionally, the active sites for the ORR were

claimed to be the nitrogen-activated carbon atoms, on which the ORR proceeded by a surface-confined redox-mediation mechanism in both acid and alkaline media [24,26]. In this work, we will use polyaniline as the carbon source to synthesize the NOMC catalysts and to optimize the pyrolysis conditions. In order to improve the electrocatalytic activity, the as-prepared catalyst is further subjected to the $NH_3$-activation at high temperatures. Then, the nitrogen sorption isotherm, electron microscopy and X-ray photoelectron spectroscopy are used to study the microstructure and composition. The cyclic voltammetry and rotating-ring-disk electrode methods are used to investigate the electrochemical behavior for the ORR.

## 2. Results and Discussion

Figure 1 shows the nitrogen sorption isotherm of the as-synthesized carbon materials. It is seen that all curves show a similar shape of the typical Type-IV isotherm, which indicates the mesoporous nature of the synthesized carbon (see Figure S1). Pore parameters are then extracted from the isotherms and listed in Table 1. It is seen that the specific surface area increases from 470 to 629 $m^2 \cdot g^{-1}$ with increasing the pyrolysis temperature from 800 to 1000 °C, which can be ascribed to the deepened decomposition in this course. Then, a further increase in the pyrolysis temperature to 1100 °C results in a decrease in the specific surface area, which may be linked to the collapse of the carbon framework. A similar trend is also seen in the specific pore volume, which reaches the highest value of 0.81 $cm^{-3} \cdot g^{-1}$ at 1000 °C. It is noted that the post-treatment in $NH_3$ yields a dramatic increase in the specific surface area (1312 $m^2 \cdot g^{-1}$), which can be attributed to the gasification of amorphous carbon and the consequent formation of micro-/meso-pores in the active atmosphere [27–29].

**Table 1.** Pore features of the synthesized carbon materials.

| Samples | $A_{BET}$/$m^2 \cdot g^{-1}$ | $A_{MP}$/$m^2 \cdot g^{-1}$ | $D_{BJH}$/nm | $V$/$cm^3 \cdot g^{-1}$ |
|---|---|---|---|---|
| **C-PA-800** | 470 | 67 | 5.4 | 0.58 |
| **C-PA-900** | 569 | 41 | 5.9 | 0.80 |
| **C-PA-1000** | 629 | 132 | 6.1 | 0.81 |
| **C-PA-1100** | 517 | 61 | 5.9 | 0.67 |
| **C-PA-1000-$NH_3$** | 1312 | 229 | 5.9 | 1.73 |

The surface composition is characterized by XPS, for which the survey spectra are shown in Figure S2. The content of the main elements are qualified and listed in Table 2. It is found that both the pyrolysis temperature and $NH_3$-activation yield a significant effect on the nitrogen content. First, the nitrogen content shows a monotonic decrease from 5.07 to 1.25 at. % with increasing the pyrolysis temperature from 800 to 1100 °C, which should be attributed to the enhanced decomposition of the nitrogen-containing functional groups at higher temperatures. Second, the nitrogen content is 2.20 at. % for C-PA-1000 and 3.15 at. % for C-PA-1000-$NH_3$, indicating that the nitrogen doping can be enhanced by the pyrolysis in the nitrogen-containing active gases. The change in the surface composition is expected to yield effects on the electrocatalysis, as discussed below.

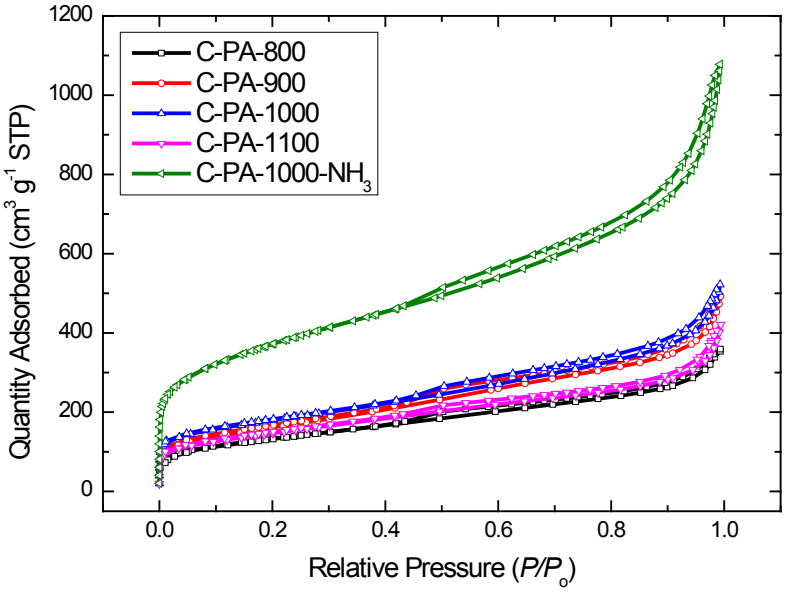


**Figure 1.** Nitrogen sorption isotherms of the synthesized carbon materials (STP: standard temperature and pressure).

**Table 2.** Elemental composition (at. %) of the synthesized carbon materials.

| Samples | C | N | O | N:C |
|---|---|---|---|---|
| C-PA-800 | 86.63 | 5.07 | 5.33 | 0.057 |
| C-PA-900 | 92.03 | 3.13 | 4.40 | 0.034 |
| C-PA-1000 | 93.45 | 2.20 | 3.91 | 0.024 |
| C-PA-1100 | 94.88 | 1.25 | 3.57 | 0.013 |
| C-PA-1000-NH3 | 94.32 | 3.15 | 2.33 | 0.033 |

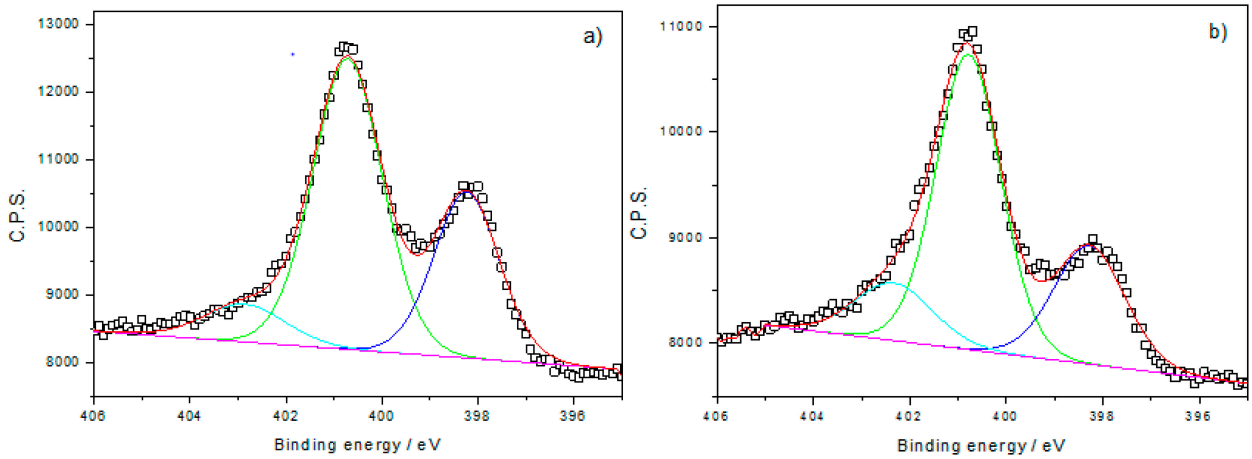


**Figure 2.** *Cont.*

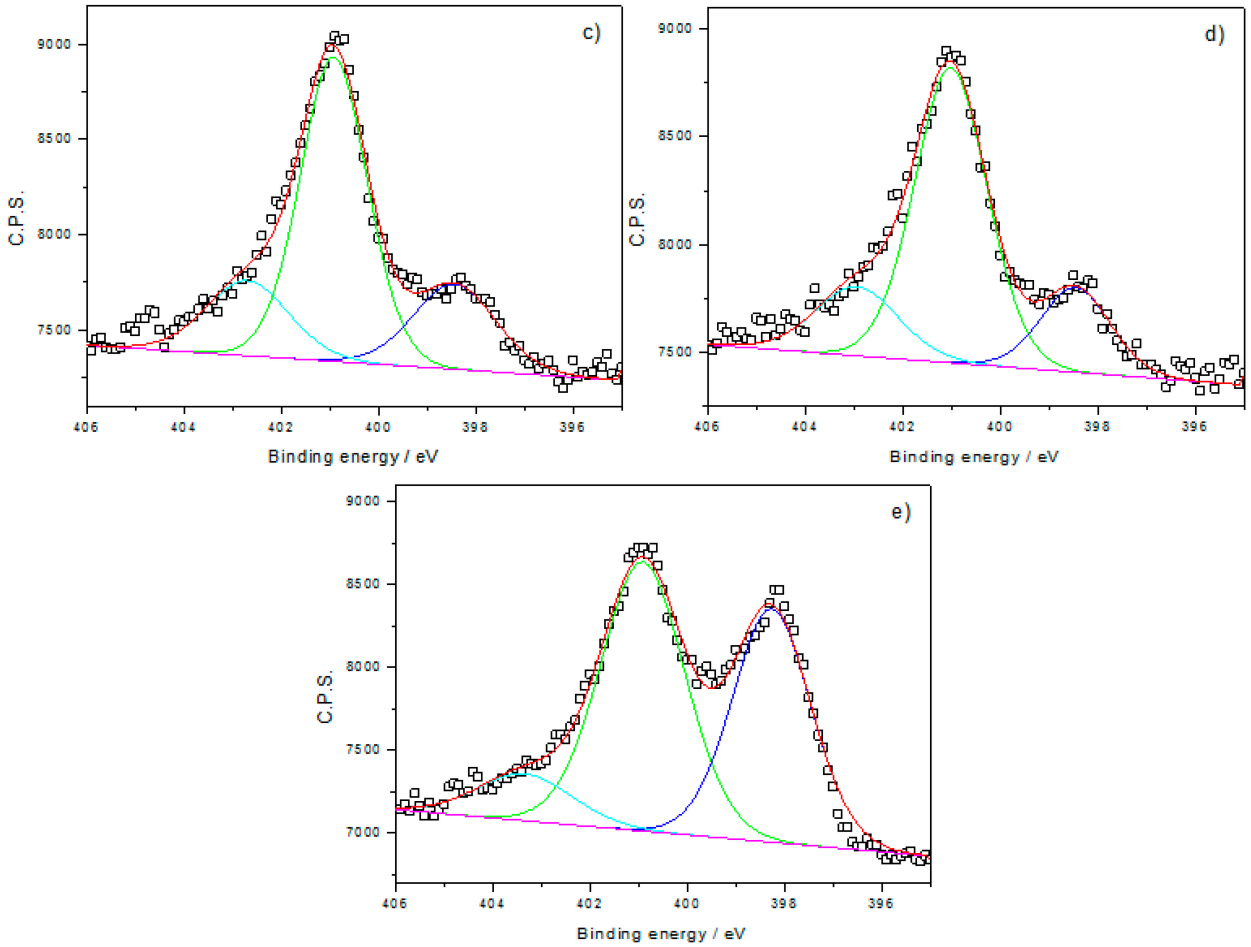


**Figure 2.** N 1s peak and the peak fitting results of the following materials: (**a**) C-PA-800; (**b**) C-PA-900; (**c**) C-PA-1000; (**d**) C-PA-1100; and (**e**) C-PA-1000-$NH_3$. The unit of *y*-axis unit is counts per second (C.P.S.).

Figure 2 shows the high-resolution XPS spectra of N 1s. These spectra can be deconvoluted to three peaks based on the binding energy: 398.4 ± 0.2, 401.0 ± 0.1 and 401.5–404 eV, which respectively correspond to pyridinic-nitrogen, graphitic-nitrogen and nitrogen-oxide [30,31]. Then, the content of each species is seen in Table 3. It is seen that the graphitic nitrogen is the predominant component among the three species, of which the content slightly increases with the pyrolysis temperature. In comparison, the content of the pyridinic-nitrogen decreases from 31.88% to 17.90% with increasing the pyrolysis temperature from 800 to 1100 °C. These results are consistent with the previous findings that the graphitic nitrogen is the most stable nitrogen species at high temperatures [32,33]. Finally, C-PA-1000-$NH_3$ shows an extraordinarily high content of pyridinic-nitrogen (40.31%), which should be attributed to the nitrogen doping at the edge of the graphite plane during the $NH_3$-etching process. It seems that the content of the graphitic nitrogen decreases to 49.88% in the etching process; however, it should be noted that the "absolute" content of this species remains unchanged, as compared with the un-etched one, by considering the total nitrogen content (see Table 2).

**Table 3.** Content of each nitrogen component (%) of the synthesized carbon materials.

| Samples | Pyridinic-N | Graphitic-N | O-N |
|---|---|---|---|
| C-PA-800 | 31.88 | 59.10 | 9.02 |
| C-PA-900 | 26.42 | 59.55 | 14.04 |
| C-PA-1000 | 20.90 | 60.62 | 18.48 |
| C-PA-1100 | 17.90 | 64.72 | 17.38 |
| C-PA-1000-$NH_3$ | 40.31 | 49.88 | 9.81 |

In our previous work, the relationship has been well established between the content of the nitrogen-activated carbon and the electrocatalytic activity for ORR [24]. In line with this understanding, the curve fitting of high-resolution C1s peak is performed (see Figure S3), and the results are listed in Table 4. It is found that the content of the nitrogen-activated carbon slightly increases with increasing pyrolysis temperature from 800 to 1000 °C and then decreases at 1100 °C. Additionally, C-PA-1000-$NH_3$ shows the highest content of nitrogen-activated carbon among all of the carbon materials. The ORR performance is expected to follow this change in content, as seen below.

**Table 4.** Content of each carbon component (%) of the synthesized carbon materials.

| Samples | C–C=C | C–N | C–O/C=N | C=O | COOH |
|---|---|---|---|---|---|
| C-PA-800 | 65.58 | 13.19 | 14.39 | 5.52 | 1.33 |
| C-PA-900 | 68.29 | 15.60 | 8.81 | 5.46 | 1.84 |
| C-PA-1000 | 68.84 | 18.51 | 7.53 | 3.85 | 1.28 |
| C-PA-1100 | 73.60 | 15.11 | 6.10 | 3.71 | 1.48 |
| C-PA-1000-$NH_3$ | 67.98 | 20.49 | 7.84 | 1.65 | 2.04 |

Figure 3 shows the CV curves in Ar-saturated 0.10 M KOH. It is seen that all of the curves are similar in shape with large capacitance currents, and broad symmetrical redox peaks are found in the potential range of 0 to 0.9 V. It is understandable that a large capacitance current should result from the high specific surface area, and the pseudocapacitance current is associated with the chemical adsorption of $OH^-$ onto the enriched redox couples. Basically, the capacitance current shows a volcano-shape relationship with the pyrolysis temperature, which first increases and then dramatically decreases at temperatures of 1100 °C. Notably, C-PA-1000-$NH_3$ shows the largest capacitance current. Such a change can be rationalized as a result of the specific surface area (*vide supra*). In comparison, the pseudocapacitance current shows a monotonic decrease with increasing pyrolysis temperature. Additionally, this result should be associated with the deepened decomposition of the electrochemically-active functional groups (like nitrogen-containing species) on the surface at higher temperatures. In line with the above analysis, C-PA-1000-$NH_3$ should yield the largest pseudocapacitance/capacitance currents due to its extraordinarily high specific surface area and nitrogen content. However, the increase in the capacitance current is not that large, and the pseudocapacitance current does not increase. This seeming contradiction may be understandable by considering the pore structure. The $NH_3$ post-treatment can effectively gasify/etch the amorphous carbon, leaving enriched micropores in the bulk. Additionally, these pores may not be fully utilized due to the lack of contact with the liquid electrolyte.

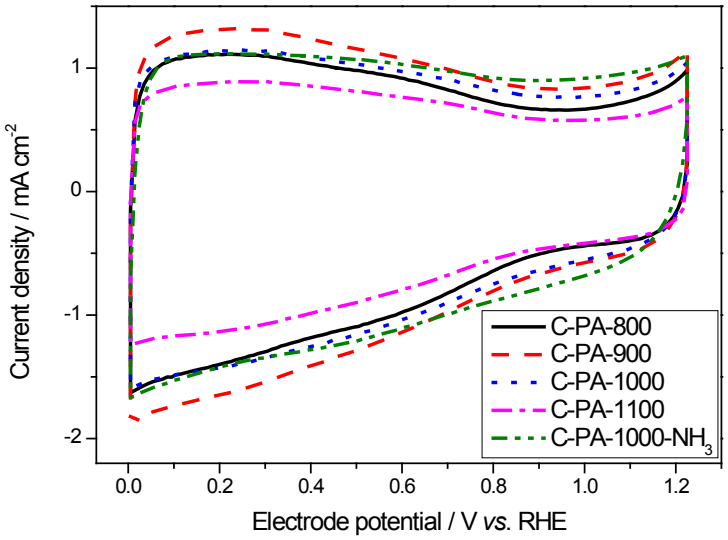


**Figure 3.** Cyclic voltammograms of the carbon materials in Ar-saturated 0.10 M KOH solution. RHE, reversible hydrogen electrode.

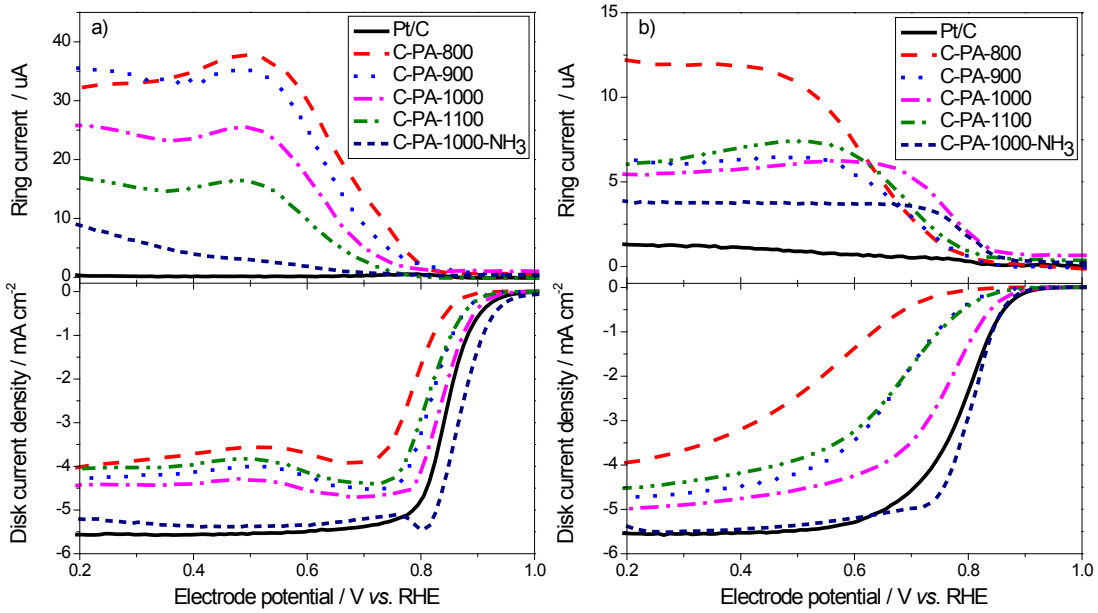


**Figure 4.** Ring (top) and disk (bottom) currents for the RRDE tests of the carbon materials: (**a**) $O_2$-saturated 0.10 M KOH solution; (**b**) $O_2$-saturated 0.10 M $HClO_4$ solution.

Figure 4 shows the polarization curves of the carbon materials in $O_2$-saturated 0.10 M KOH and 0.10 M $HClO_4$ solutions. Figure 4a shows that in alkaline media, the electrocatalytic activity shows a volcano-shape relationship, which increases with the pyrolysis temperature from 800 to 1000 °C and then decreases at 1100 °C. The same trend is further seen in the change of the yield of hydrogen peroxide and electron transfer number (see Figure S4a). Increasing the pyrolysis temperature lowers the yield of hydrogen peroxide, and thereby, selectively favors the 4-e reduction of oxygen. Such a trend in the electrocatalytic activity and selectivity correlates well with the change in the content of nitrogen-activated carbon and the specific surface area (*vide supra*). These findings further confirm that the active sites for the ORR should be the nitrogen-activated carbon atoms [24,26]. In acid media, the change in the electrocatalytic activity is similar to that in alkaline media (Figure 4b), revealing that

the active site should remain substantially the same in a wide range of pH. Finally, it is noted that for C-PA-1000-$NH_3$, both the activity and the selectivity are considerably improved upon $NH_3$-activation. This result quantitatively agrees with the change in the specific surface area and the content of nitrogen-activated carbon, as discussed above. However, it seems irrational to directly correlate the small increase in the nitrogen-activated carbon (Table 4) with the extremely high activity and low $H_2O_2$ yield. The mechanism has not been fully understood yet, but the reason may be associated with high content of the pyridinic-nitrogen after the $NH_3$ treatment.

## 3. Experimental Section

### *3.1. Materials Preparation*

Nitrogen-doped ordered mesoporous carbon (NOMC) was synthesized by a modified nanocasting method [24]. The process is briefly described as follows. (i) Synthesis of the template SBA-15 [34]: An aqueous mixture, consisting of Pluronic P123, HCl and tetraethoxysilane, was stirred for 20 h at 35 °C and then hydrothermally treated at 100 °C for 24 h. The resultant powders were calcined in air at 550 °C for 6 h, and SBA-15 was finally obtained. (ii) Impregnation of the carbon precursor: Aniline was impregnated into SBA-15 by the vaporization-capillary condensation method [24]. Then, the monomer was polymerized upon adding $FeCl_3$ to form polyaniline (PA). (iii) Pyrolysis and template removal: The resultant powders were then subjected to the pyrolysis at high temperatures (800, 900, 1000, 1100 °C) for 3 h in argon, respectively. Finally, the carbon catalyst was obtained by removing the silicate template by boiling in 10 M NaOH solution for 24 h. The samples were referred to as C-PA-X. Here, X refers to the pyrolysis temperature, *viz*. 800, 900, 1000 and 1100. In addition, the sample C-PA-1000 was heat-treated again at 1000 °C in ammonia for 30 min, which was labeled as C-PA-1000-$NH_3$.

### *3.2. Physical Characterizations*

X-ray photoelectron spectroscopy (XPS, Physical Electronics PHI 5600, Chanhassen, MN, USA) measurement was carried out with a multi-technique system using an Al monochromatic X-ray at a power of 350 W. Transmission electron microscopy (TEM) was performed on an FEI Tecnai G2 F20 S-TWIN (Hillsboro, OR, USA) operated at 200 kV. Nitrogen adsorption/desorption isotherms were measured at 77 K using a Micromeritics TriStar II 3020 analyzer (Norcross, GA, USA). The total surface area was analyzed with the well-established Brunauer–Emmett–Teller (BET) method; the microporous surface area was obtained with the MP (micropore) method (*t*-plot method); and the pore size distribution was analyzed by the Barrett–Joyner–Halenda (BJH) method.

### *3.3. Electrochemical Characterization*

The electrochemical behavior of the catalyst was characterized by the cyclic voltammetry (CV) and linear sweeping voltammetry (LSV) using a three-electrode cell with an electrochemical work station Zennium (Zahner, Germany) at room temperature (25 °C). A platinum wire and a double-junction Ag/AgCl reference electrode were used as the counter and reference electrodes, respectively. The working electrode was a rotating ring-disk electrode (RRDE, glassy carbon disk: 5.0 mm in diameter; platinum ring: 6.5 mm inner diameter and 7.5 mm outer diameter). The thin-film electrode on the disk

was prepared as follows. Ten milligrams of the catalyst were dispersed in 1.0 mL Nafion/ethanol (0.84 wt. % Nafion) by sonication for 120 min. Then, 10 μL of the dispersion were transferred onto the glassy carbon disk by using a pipette, yielding the catalyst loading of 0.50 $mg \cdot cm^{-2}$. The ORR activity of the Pt/C catalyst (HiSPEC4000, Johnson Matthey, London, UK) with the metal loading of 20 $\mu g \cdot cm^{-2}$ was collected for comparison.

The electrolyte solution, 0.10 M KOH, was first bubbled with argon for 60 min. Then, a CV test was conducted at 20 $mV \cdot s^{-1}$ in the potential range between 0 and 1.23 V (*vs.* reversible hydrogen electrode, RHE) for 20 cycles. If not specified, the LSV curve was collected by scanning the disk potential from 1.2 down to 0 V at 5 $mV \cdot s^{-1}$ in the oxygen-saturated electrolyte solution under 1600 rpm, from which the ORR polarization curve was extracted by subtracting the capacitive current. During the collection, the potential of the ring was set to be 0.5 V (*vs.* RHE) to determine the yield of hydrogen peroxide.

The electron-transfer number ($n$) and hydrogen peroxide yield ($H_2O_2$%) in the ORR were calculated from the following equations:

$$n = \frac{4|i_d|}{|i_d| + i_r/N} \quad (1)$$

$$H_2O_2(\%) = \frac{2i_r/N}{|i_d| + i_r/N} \times 100 \quad (2)$$

where $i_d$ is the disk current, $i_r$ is the ring current and $N$ is the collection efficiency (=20.50%).

## 4. Conclusions

Nitrogen-doped ordered mesoporous carbon was synthesized by the modified nanocasting method with high electrocatalytic activities to the ORR in both acid and alkaline media. The results revealed that both the pyrolysis temperature and the $NH_3$-activation yielded significant effects on the specific surface area, nitrogen doping and, thus, the electrocatalytic activity, as well. First, the pyrolysis temperature yielded a volcano-shape relationship with the specific surface area and the content of the nitrogen-activated carbon. Additionally, it was found that such a change could be correlated with the electrocatalytic activity to the ORR, revealing the importance of the specific surface area and the chemical nature of the active sites. Second, the post-treatment in $NH_3$ could further increase the specific surface and enhance the nitrogen doping, which thereby improved the electrocatalytic activity and selectivity to the ORR. Additionally, the C-PA-1000-$NH_3$ catalyst outperformed the Pt/C one in both acid and alkaline media, which make it promising to be applied in fuel cells.

## Acknowledgments

The work described in this paper was jointly supported by the National Natural Science Foundation of China (No. 21476087), the Pearl River S&T Nova Program of Guangzhou (No. 2013J2200041), the Science & Technology Research Project of Guangdong Province (No. 2014A010105041), the Guangdong Natural Science Foundation (No. S2013010012469) and the Innovation Project of Guangdong Department of Education (No. 2014KTSCX016).

## Author Contributions

K.W. and Z.P.Y. performed the experiment and analyzed the data; K.W. and Z.X.L. wrote the paper.

## Conflicts of Interest

The authors declare no conflicts of interest.

## References

1. Job, N.; Lambert, S.; Zubiaur, A.; Cao, C.; Pirard, J.P. Design of Pt/carbon xerogel catalysts for pem fuel cells. *Catalysts* **2015**, *5*, 40–57.
2. Jia, Q.; Liang, W.; Bates, M.K.; Mani, P.; Lee, W.; Mukerjee, S. Activity descriptor identification for oxygen reduction on platinum-based bimetallic nanoparticles: *In situ* observation of the linear composition-strain-activity relationship. *ACS Nano* **2015**, *9*, 387–400.
3. Ye, T.N.; Lv, L.B.; Li, X.H.; Xu, M.; Chen, J.S. Strongly veined carbon nanoleaves as a highly efficient metal-free electrocatalyst. *Angew. Chem. Int. Ed.* **2014**, *53*, 6905–6909.
4. Wu, G.; Zelenay, P. Nanostructured nonprecious metal catalysts for oxygen reduction reaction. *Acc. Chem. Res.* **2013**, *46*, 1878–1889.
5. Zhang, Y.; Zhuang, X.D.; Su, Y.Z.; Zhang, F.; Feng, X.L. Polyaniline nanosheet derived B/N co-doped carbon nanosheets as efficient metal-free catalysts for oxygen reduction reaction. *J. Mater. Chem. A* **2014**, *2*, 7742–7746.
6. Su, D.S.; Perathoner, S.; Centi, G. Nanocarbons for the development of advanced catalysts. *Chem. Rev.* **2013**, *113*, 5782–5816.
7. Wang, H.L.; Dai, H.J. Strongly coupled inorganic-nano-carbon hybrid materials for energy storage. *Chem. Soc. Rev.* **2013**, *42*, 3088–3113.
8. Gong, K.; Du, F.; Xia, Z.; Durstock, M.; Dai, L. Nitrogen-doped carbon nanotube arrays with high electrocatalytic activity for oxygen reduction. *Science* **2009**, *323*, 760–764.
9. Yang, S.; Feng, X.; Wang, X.; Müllen, K. Graphene-based carbon nitride nanosheets as efficient metal-free electrocatalysts for oxygen reduction reactions. *Angew. Chem. Int. Ed.* **2011**, *50*, 5339–5343.
10. He, W.; Jiang, C.; Wang, J.; Lu, L. High-rate oxygen electroreduction over graphitic-n species exposed on 3D hierarchically porous nitrogen-doped carbons. *Angew. Chem. Int. Ed.* **2014**, *53*, 9503–9507.
11. Zhu, Y.; Zhang, B.; Liu, X.; Wang, D.W.; Su, D.S. Unravelling the structure of electrocatalytically active Fe–N complexes in carbon for the oxygen reduction reaction. *Angew. Chem. Int. Ed.* **2014**, *53*, 10673–10677.
12. Sun, X.; Song, P.; Zhang, Y.; Liu, C.; Xu, W.; Xing, W. A class of high performance metal-free oxygen reduction electrocatalysts based on cheap carbon blacks. *Sci. Rep.* **2013**, *3*, 2505.
13. Silva, R.; Voiry, D.; Chhowalla, M.; Asefa, T. Efficient metal-free electrocatalysts for oxygen reduction: Polyaniline-derived N- and O-doped mesoporous carbons. *J. Am. Chem. Soc.* **2013**, *135*, 7823–7826.

14. Ramaswamy, N.; Tylus, U.; Jia, Q.; Mukerjee, S. Activity descriptor identification for oxygen reduction on nonprecious electrocatalysts: Linking surface science to coordination chemistry. *J. Am. Chem. Soc.* **2013**, *135*, 15443–15449.
15. Liang, H.W.; Wei, W.; Wu, Z.S.; Feng, X.; Mullen, K. Mesoporous metal-nitrogen-doped carbon electrocatalysts for highly efficient oxygen reduction reaction. *J. Am. Chem. Soc.* **2013**, *135*, 16002–16005.
16. Liu, G.; Li, X.G.; Ganesan, P.; Popov, B.N. Development of non-precious metal oxygen-reduction catalysts for pem fuel cells based on N-doped ordered porous carbon. *Appl. Catal. B* **2009**, *93*, 156–165.
17. Cheon, J.Y.; Kim, T.; Choi, Y.; Jeong, H.Y.; Joo, S.H. Ordered mesoporous porphyrinic carbons with very high electrocatalytic activity for the oxygen reduction reaction. *Sci. Rep.* **2013**, *3*, 2715.
18. Yin, H.; Zhang, C.; Liu, F.; Hou, Y. Hybrid of iron nitride and nitrogen-doped graphene aerogel as synergistic catalyst for oxygen reduction reaction. *Adv. Funct. Mater.* **2014**, *24*, 2930–2937.
19. Xi, P.B.; Liang, Z.X.; Liao, S.J. Stability of hemin/C electrocatalyst for oxygen reduction reaction. *Int. J. Hydrogen Energy* **2012**, *37*, 4606–4611.
20. Liang, Z.X.; Song, H.Y.; Liao, S.J. Hemin: A highly effective electrocatalyst mediating the oxygen reduction reaction. *J. Phys. Chem. C* **2011**, *115*, 2604–2610.
21. Fellinger, T.P.; Hasche, F.; Strasser, P.; Antonietti, M. Mesoporous nitrogen-doped carbon for the electrocatalytic synthesis of hydrogen peroxide. *J. Am. Chem. Soc.* **2012**, *134*, 4072–4075.
22. Sa, Y.J.; Park, C.; Jeong, H.Y.; Park, S.H.; Lee, Z.; Kim, K.T.; Park, G.G.; Joo, S.H. Carbon nanotubes/heteroatom-doped carbon core-sheath nanostructures as highly active, metal-free oxygen reduction electrocatalysts for alkaline fuel cells. *Angew. Chem. Int. Ed.* **2014**, *53*, 4102–4106.
23. Wu, G.; More, K.L.; Johnston, C.M.; Zelenay, P. High-performance electrocatalysts for oxygen reduction derived from polyaniline, iron, and cobalt. *Science* **2011**, *332*, 443–447.
24. Wan, K.; Long, G.F.; Liu, M.Y.; Du, L.; Liang, Z.X.; Tsiakaras, P. Nitrogen-doped ordered mesoporous carbon: Synthesis and active sites for electrocatalysis of oxygen reduction reaction. *Appl. Catal. B* **2015**, *165*, 566–571.
25. Long, G.F.; Wan, K.; Liu, M.Y.; Li, X.H.; Liang, Z.X.; Piao, J.H. Effect of pyrolysis conditions on nitrogen-doped ordered mesoporous carbon electrocatalysts. *Chin. J. Catal.* **2015**, doi:10.1016/S1872-2067(15)60912-3.
26. Wan, K.; Yu, Z.P.; Li, X.H.; Liu, M.Y.; Yang, G.; Piao, J.H.; Liang, Z.X. PH effect on electrochemistry of nitrogen-doped carbon catalyst for oxygen reduction reaction. *ACS Catal.* **2015**, *5*, 4325–4332.
27. Meng, H.; Larouche, N.; Lefèvre, M.; Jaouen, F.; Stansfield, B.; Dodelet, J.-P. Iron porphyrin-based cathode catalysts for polymer electrolyte membrane fuel cells: Effect of $NH_3$ and Ar mixtures as pyrolysis gases on catalytic activity and stability. *Electrochim. Acta* **2010**, *55*, 6450–6461.
28. Zhao, Y.; Watanabe, K.; Hashimoto, K. Self-supporting oxygen reduction electrocatalysts made from a nitrogen-rich network polymer. *J. Am. Chem. Soc.* **2012**, *134*, 19528–19531.
29. Liang, H.W.; Zhuang, X.; Bruller, S.; Feng, X.; Mullen, K. Hierarchically porous carbons with optimized nitrogen doping as highly active electrocatalysts for oxygen reduction. *Nat. Commun.* **2014**, *5*, 4973.

30. Chen, S.; Bi, J.Y.; Zhao, Y.; Yang, L.J.; Zhang, C.; Ma, Y.W.; Wu, Q.; Wang, X.Z.; Hu, Z. Nitrogen-doped carbon nanocages as efficient metal-free electrocatalysts for oxygen reduction reaction. *Adv. Mater.* **2012**, *24*, 5593–5597.
31. Hu, Y.; Jensen, J.O.; Zhang, W.; Cleemann, L.N.; Xing, W.; Bjerrum, N.J.; Li, Q. Hollow spheres of iron carbide nanoparticles encased in graphitic layers as oxygen reduction catalysts. *Angew. Chem. Int. Ed.* **2014**, *53*, 3675–3679.
32. Geng, D.; Chen, Y.; Chen, Y.; Li, Y.; Li, R.; Sun, X.; Ye, S.; Knights, S. High oxygen-reduction activity and durability of nitrogen-doped graphene. *Energ. Environ. Sci.* **2011**, *4*, 760–764.
33. Favaro, M.; Perini, L.; Agnoli, S.; Durante, C.; Granozzi, G.; Gennaro, A. Electrochemical behavior of n and ar implanted highly oriented pyrolytic graphite substrates and activity toward oxygen reduction reaction. *Electrochim. Acta* **2013**, *88*, 477–487.
34. Zhao, D.Y.; Feng, J.L.; Huo, Q.S.; Melosh, N.; Fredrickson, G.H.; Chmelka, B.F.; Stucky, G.D. Triblock copolymer syntheses of mesoporous silica with periodic 50 to 300 angstrom pores. *Science* **1998**, *279*, 548–552.